

Multifunctional Two-dimensional van der Waals Janus Magnet Cr-based Dichalcogenide Halides

Yusheng Hou^{1,#,*}, Feng Xue^{2,#}, Liang Qiu¹, Zhe Wang³ and Ruqian Wu^{4,*}

¹ Guangdong Provincial Key Laboratory of Magnetoelectric Physics and Devices, Center for Neutron Science and Technology, School of Physics, Sun Yat-Sen University, Guangzhou, 510275, China

² State Key Laboratory of Low-Dimensional Quantum Physics, Department of Physics, Tsinghua University, Beijing 100084, China and Frontier Science Center for Quantum Information, Beijing 100084, China

³ State Key Laboratory of Surface Physics and Key Laboratory for Computational Physical Sciences (MOE) and Department of Physics, Fudan University, Shanghai 200433, China

⁴ Department of Physics and Astronomy, University of California, Irvine, CA 92697-4575, USA

Contributed equally to this work

Corresponding authors (*): houysh@mail.sysu.edu.cn; wur@uci.edu

Abstract

Two-dimensional van der Waals Janus materials and their heterostructures offer fertile platforms for designing fascinating functionalities. Here, by means of systematic first-principles studies on van der Waals Janus monolayer Cr-based dichalcogenide halides CrYX ($Y=\text{S, Se, Te}$; $X=\text{Cl, Br, I}$), we find that CrSX ($X=\text{Cl, Br, I}$) are the very desirable high T_C ferromagnetic semiconductors with an out-of-plane magnetization. Excitingly, by the benefit of the large magnetic moments on ligand S^{2-} anions, the sought-after large-gap quantum anomalous Hall effect and sizable valley splitting can be achieved through the magnetic proximity effect in van der Waals heterostructures $\text{CrSBr}/\text{Bi}_2\text{Se}_3/\text{CrSBr}$ and $\text{MoTe}_2/\text{CrSBr}$, respectively. Additionally, we show that large Dzyaloshinskii-Moriya interactions give rise to skyrmion states in CrTeX ($X=\text{Cl, Br, I}$) under external magnetic fields. Our work reveals that two-dimensional Janus magnet Cr-based dichalcogenide halides have appealing multifunctionalities in the applications of topological electronic and valleytronic devices.

Keywords: Two-dimensional van der Waals magnets, Janus materials, quantum anomalous Hall effect, valley splitting, magnetic skyrmion

INTRODUCTION

The discovery of ferromagnetism at a finite temperature in atomically thin van der Waals (vdW) monolayers (MLs) ¹⁻³ has spurred a surge of experimental and theoretical interests in understanding the two-dimensional (2D) magnetism and furthermore in producing emergent functionalities in 2D vdW heterostructures⁴⁻⁹. Fundamentally, the well-known Mermin-Wagner theorem based on the isotropic Heisenberg exchange model ¹⁰ suggested the absence of either FM or antiferromagnetic (AFM) order in 2D systems at nonzero temperature, and hence the early findings of FM order in CrI₃ ML ¹ and Cr₂Ge₂Te₆ bilayer ¹¹ were rather surprising. Recent studies indicated that magnetic anisotropies play a major role in the establishment of their long-range magnetic ordering. The main advantage of these 2D magnetic vdW materials is their integrability with other vdW functional materials. Through the magnetic proximity effect, many spintronic, valleytronic and optoelectronic properties can be achieved in heterostructures by stacking diverse 2D vdW MLs or ultrathin films ^{5,7,8}. For example, the quantum anomalous Hall effect (QAHE) and axion insulator phase can be realized by integrating 2D FM semiconductors with thin films of topological insulators ^{8,12-15}. When transition metal dichalcogenide (TMDC) MLs are in contact with 2D FM semiconductors, a valley splitting can be produced for valleytronic and optoelectronic manipulations ⁷, as recently observed in WSe₂/CrI₃ ¹⁶. Obviously, it is beneficial to have large spin polarization in the outer anions of 2D FM MLs to maximize the magnetic proximity effect.

Recently, Janus 2D materials have attracted increasing attention ^{17,18} since TMDC Janus ML MoSSe was successfully fabricated by controlling the reaction conditions in experiments ¹⁹. Due to the feasibility of selecting a suitable pair of anions, Janus 2D materials add an extra dimension for the rational design of 2D vdW MLs with desired properties. For example, because the out-of-plane symmetry is broken, 2D Janus CrGe(Se,Te)₃, CrXTe ($X=S, Se$) and manganese dichalcogenide MLs may possess large Dzyaloshinskii-Moriya interaction (DMI) and thus can host magnetic skyrmions ²⁰⁻²³. Besides, Janus structure as electrodes in Li-ion batteries may have good performance due to its structural asymmetry ²⁴. Several theoretical studies ²⁵⁻²⁸ predicted that Janus MLs, such as VSSe ²⁷, a Janus structure of the FM VSe₂ ^{2,29}, have FM order up to room-temperature. Although 2D Janus magnets' own properties have been widely investigated, their heterostructures with other vdW functional materials, such as TMDC MLs and three-dimensional (3D) topological insulator thin films, remain underexplored ^{17,18}. Moreover, the formation of complex magnetic patterns in 2D heterostructures due to the competition among Heisenberg exchange, magnetic anisotropy, DMI and external magnetic field is rarely discussed.

In this work, we systematically study the electronic and magnetic properties of vdW Janus ML Cr-based dichalcogenide halides CrYX ($Y=S, Se, Te; X=Cl, Br, I$) using first-principles calculations. This is partially inspired by the experimental observation of high-temperature (~ 200 K) ferromagnetism in 1T-CrTe₂ ML ³⁰⁻³⁴. We identify that CrSX ($X=Cl, Br, I$) are the very attractive out-of-plane FM semiconductors with high Curie

temperatures (~ 176 K) and large magnetic moments on S^{2-} anions. Excitingly, through the magnetic proximity effect, the sought-after large-gap QAHE can be achieved in CrSBr/Bi₂Se₃/CrSBr. For the same reason, a sizable valley splitting of 37.9 meV, corresponding to a magnetic field of 379 Tesla³⁵, can be generated in MoTe₂/CrSBr. Furthermore, we find that large DMI leads to magnetic skyrmion states in CrTeX ($X=Cl, Br, I$) under an appropriate external magnetic field by virtue of Monte Carlo (MC) simulations. Our work highlights the remarkable multifunctionalities of these 2D vdW Janus ML magnets that are promising for applications in the next-generation topotronic and valleytronic devices.

RESULTS

Electronic and magnetic properties of CrYX ML

Fig. 1a shows the crystal structure of Janus ML CrYX ($Y=S, Se, Te; X=Cl, Br, I$). Magnetic Cr³⁺ cations form a triangular lattice and are sandwiched by Y^{2-} and X^- anions. Similar to CrI₃ and Cr₂Ge₂Te₆ MLs^{1,11}, Cr³⁺ cations in CrYX are surrounded by the distorted edge-shared octahedrons formed by Y^{2-} and X^- anions, which implies FM nearest neighbor (NN) exchange interactions. As a direct result of different sizes of Y^{2-} and X^- anions, CrSCl and CrTeI have the smallest and largest in-plane lattice constants (Supplementary Table 1), respectively. Since no imaginary frequency is found in the calculated phonon spectra of all CrYX MLs (Supplementary Fig. 1), they should be dynamically stable.

To explore the magnetic ground states of CrYX MLs, we consider a spin Hamiltonian consisting of Heisenberg exchange interactions, DMI and single ion anisotropy (SIA).

This spin Hamiltonian is in the form of ^{21,22}

$$H = J_1 \sum_{\langle ij \rangle} \mathbf{S}_i \cdot \mathbf{S}_j + J_2 \sum_{\langle\langle ij \rangle\rangle} \mathbf{S}_i \cdot \mathbf{S}_j + J_3 \sum_{\langle\langle\langle ij \rangle\rangle\rangle} \mathbf{S}_i \cdot \mathbf{S}_j + \sum_{\langle ij \rangle} \mathbf{D}_{ij} \cdot (\mathbf{S}_i \times \mathbf{S}_j) - A \sum_i (S_i^z)^2 \quad (1).$$

Here, \mathbf{S}_i is the normalized spin vector at site i ; J_1 , J_2 and J_3 are NN, second-NN and third-NN Heisenberg exchange parameters, respectively; $\mathbf{D}_{ij}=(D_x, D_y, D_z)$ is the NN DMI vector and A is the SIA parameter. The Heisenberg exchange parameters J_i ($i=1, 2, 3$), NN DM vector \mathbf{D}_1 and SIA parameter A from DFT calculations are tabulated in Supplementary Table 2. As expected, the NN J_1 is FM and dominates over the second-NN J_2 and third-NN J_3 for all CrYX (Fig. 1b). Since DMI is directly related to the spin-orbit coupling (SOC) ³⁶, the magnitude of the NN DMI vector, $|\mathbf{D}_1| = \sqrt{D_x^2 + D_y^2 + D_z^2}$, increases when Y (X) goes from S (Cl) to Te (I), as shown in Fig. 1c. It is interesting that $|\mathbf{D}_{1,\parallel}|/|J_1|$ ($\mathbf{D}_{1,\parallel}$, the inplane component of \mathbf{D}_1) has a similar trend to $|\mathbf{D}_1|$ when Y (X) varies (Fig. 1c). Particularly, $|\mathbf{D}_{1,\parallel}|/|J_1|$ of CrTeX ($X=\text{Cl, Br, I}$) is in the typical range of 0.1-0.2 that is known to generate magnetic skyrmions ³⁷. Lastly, CrSX ($X=\text{Cl, Br, I}$) and CrSeI have an out-of-plane SIA while the other five of CrYX have an in-plane SIA (Fig. 1d). Note that the present results of NN FM Heisenberg exchange interactions and in-plane SIAs of CrSeBr and CrTeI Janus MLs are consistent with those obtained in a previous theoretical study ³⁸.

Owing to the competition between Heisenberg exchange interactions, DMI and SIA, MC simulations reveal that CrYX exhibits very rich magnetic ground configurations

(Fig. 1e). It has been reported that magnetic ground state of 2D magnets is mainly determined by a critical dimensionless factor $|A|K/\mathbf{D}_{//}^2$ (K , the stiffness parameter originating from FM Heisenberg exchange interactions)³⁹. A large $|A|K/\mathbf{D}_{//}^2$ yields a FM ground state, while a small one results in a spiral ground state³⁹. First, CrSY ($Y=\text{Cl, Br, I}$) MLs have small DMI, out-of-plane SIA and hence an out-of-plane FM ground state with a Curie temperature up to 176 K (Supplementary Fig. 2). CrSeCl also has a FM ground state, but its magnetization is in plane due to its negative SIA. Second, CrSeBr and CrSeI have medium DMI, small SIA, and hence small $|A|K/\mathbf{D}_{//}^2$. Therefore, they have a spin spiral ground state with a large periodic length. Finally, CrTeX ($X=\text{Cl, Br, I}$) MLs have both large DMI and SIA. Their magnetic ground states have wormlike domains, similar to what was found in the previous studies of 2D Janus manganese dichalcogenides²⁰.

Considering the needed semiconducting nature of vdW ferromagnets for engineering emergent physical properties via the magnetic proximity effect in heterostructures^{7,13,16}, we first analyze the electronic properties of CrSX ($X=\text{Cl, Br, I}$) MLs which have a FM ground state and out-of-plane magnetic anisotropy. Band structures in Figs. 2a-2c show that all CrSX MLs are indirect-gap semiconductors. As the electronegativity weakens from Cl to Br and to I, the band gaps of CrSX decrease from 2.17 eV (CrSCl) to 1.77 eV (CrSBr) and to 0.81 eV (CrSI). The curves of density of state (Supplementary Fig. 3) suggest that the conduction bands mainly come from the d states of Cr while the valence bands have mixtures of Cr, S and X states. Besides, the d - p hybridization

between Cr and S atoms is stronger than that between Cr and X atoms near the Fermi level.

As the magnetic ions are mostly covered by nonmagnetic anions in vdW FM semiconductors, the spin polarization of the outer layer is typically very small. The magnetic proximity effect is hence weak in most vdW heterostructures. Interestingly, the magnetic moments on S^{2-} anion are about $0.14 \mu_B/S$ in CrSX MLs, the largest for 2D FM semiconductors reported so far (Fig. 3c) ^{1,11,40-45}. Especially, this magnetic moment is much larger than that of I^{2-} anions in CrI₃ ^{7,13,16,46-49}, suggesting that CrSX may have a significant magnetic proximity effect on other vdW functional materials.

Large-gap QAHE in CrSBr/Bi₂Se₃/CrSBr vdW heterostructure

We first examine the effect of CrSX MLs on magnetizing topological surface states (TSSs) of 3D topological insulators for the realization of QAHE ⁸. We construct an vdW heterostructure with two CrSBr MLs and a six quintuple-layer Bi₂Se₃ (BS) thin film (CrSBr/BS/CrSBr). The calculated binding energies of different stacking configurations suggest that Cr³⁺ cations of CrSBr prefer to align with Bi and the S^{2-} side contacts BS thin film (Fig. 3a and more details in Supplementary Fig. 4). Our *ab initio* molecular dynamics simulations show that this CrSBr/BS/CrSBr heterostructure is thermodynamically stable (Supplementary Fig. 5). The induced spin polarization on BS penetrates through the film (Fig. 3b), with a strength twice as large as that in CrI₃/BS/CrI₃ ¹³. Fig. 3c shows the band structure of CrSBr/BS/CrSBr when the

magnetizations of top and bottom CrSBr MLs are ferromagnetically ordered. As a result of the strong magnetization in CrSBr, the system has a large band gap up to 19 meV at the Γ point, indicating its efficient magnetic proximity effect on the TSSs of BS thin film. By examining the spin components of the four bands near the Fermi level (Fig. 3d), we find that the two bands below (above) the Fermi level have the same spin-down (spin-up) components. These features clearly suggest the TSSs of the BS thin film are strongly magnetized by CrSBr.

To investigate the topological property of CrSBr/BS/CrSBr, we fit its band structure using an effective four-band model. With the bases of $\{|t, \uparrow\rangle, |t, \downarrow\rangle, |b, \uparrow\rangle, |b, \downarrow\rangle\}$, the model Hamiltonian of inversion symmetric heterostructures is written as⁵⁰

$$H(k_x, k_y) = Ak^2 + \begin{bmatrix} v_F(k_y\sigma_x - k_x\sigma_y) & M_k\sigma_0 \\ M_k\sigma_0 & -v_F(k_y\sigma_x - k_x\sigma_y) \end{bmatrix} + \begin{bmatrix} \Delta\sigma_z & 0 \\ 0 & \Delta\sigma_z \end{bmatrix} \quad (2).$$

In Eq. (2), \uparrow (\downarrow) denotes spin-up (spin-down) states; v_F , $k^2 = k_x^2 + k_y^2$ and $\sigma_{x,y,z}$ are the Fermi velocity, in-plane wave vector and Pauli matrices, respectively. The coupling between the top and bottom TSSs of BS thin film is described by $M_k = \Delta_h + Bk^2$ and Δ_h is the coupling induced gap. By fitting the DFT calculated band structure with Eq. (2) (Supplementary Fig. 6), we obtain Δ_h and Δ are 1.0 and 10.4 meV, respectively. According to the general rule proposed in Ref. 13, CrSBr/BS/CrSBr is a Chern insulator with Chern number $C_N=1$. This topological nature is further confirmed by the presence of one chiral edge state that connects the valence and conduction bands in the band structure of the one-dimensional CrSBr/BS/CrSBr nanoribbon (Fig. 3e). Taking together T_C (176 K) of the FM semiconductor CrSBr ML and the large nontrivial band

gap (19 meV, corresponding to 220 K), it is conceivable that QAHE with a high temperature can be achieved in CrSBr/BS/CrSBr.

Sizable valley splitting in CrSBr/MoTe₂ vdW heterostructure

We further explore the valley splitting of TMDC MLs in contact with CrSBr. To this end, we study the vdW heterostructure of CrSBr and MoTe₂ MLs (CrSBr/MoTe₂). Again, the calculated binding energies (Supplementary Fig. 7) indicate that the S²⁻ side of CrSBr binds to MoTe₂ (Fig. 4a). Cr³⁺ cations and S²⁻ anions sit on the top of Mo⁴⁺ cations and the hollow sites, respectively. The fat band representation in Fig. 4b shows two important features: (i) conduction bands of CrSBr locate in the gap of MoTe₂; (ii) valence and conduction bands of MoTe₂ are not much affected by CrSBr, suggesting a weak hybridization between CrSBr and MoTe₂. The Berry curvature map in the 2D Brillouin zone (Fig. 4c) shows opposite Berry curvatures in the vicinity of K₊ and K₋ valleys. These illustrate that the coupled spin and valley physics is remained in CrSBr/MoTe₂.

To quantitatively determine the valley splitting in CrSBr/MoTe₂, we adopt an energy scale³⁵, $\Delta_{\text{val}}^{c/v,\tau} = E_{\uparrow}^{c/v,\tau} - E_{\downarrow}^{c/v,-\tau}$. Here, v (c) denotes valence (conduction) bands; K_{\pm} are distinguished by index $\tau = \pm$. According to this definition, $\Delta_{\text{val}}^{v,+}$, $\Delta_{\text{val}}^{v,-}$, $\Delta_{\text{val}}^{c,+}$ and $\Delta_{\text{val}}^{c,-}$ are estimated as -37.9, -8.8, 8.6 and 8.7 meV, respectively. We see that $\Delta_{\text{val}}^{v,+}$ in CrSBr/MoTe₂ is sizable, corresponding to the valley splitting generated by a magnetic field of 379 Tesla³⁵. It is worth noting that this value is much larger than the

counterparts in CrI₃/WSe₂^{16,46,47} and CrI₃/MoTe₂⁴⁹. More remarkably, the smallest energy for the band edge vertical optical transition without spin flip in two valleys reaches a giant value of 46.5 meV. Thanks to the time reversal symmetry breaking and the nonvanishing Berry curvature, CrSBr/MoTe₂ has a nonzero anomalous hall conductivity, σ_{xy} , when Fermi level lies between the valence band maxima of K₊ and K₋ valleys (Fig. 4d). Taking together the anomalous hall conductivity and sizable valley splitting, it is conceivable that a spin- and valley-polarized Hall current can be generated in CrSBr/MoTe₂ when applying an in-plane electric field⁵¹, thus providing applications in valleytronics.

DISCUSSION

Finally, we find that CrTeX ($X=\text{Cl, Br, I}$) MLs can host magnetic skyrmion states in an external magnetic field, because of the strong SOC of Te and the symmetry reduction. This is a very attractive feature for diverse applications as discussed in the literatures for the studies of other magnetic systems⁵²⁻⁵⁴. To characterize the presence of magnetic skyrmions in MC simulations, we calculate the topological charge Q which is defined as:⁵⁵

$$Q = \frac{1}{4\pi} \int \mathbf{m} \cdot \left(\frac{\partial \mathbf{m}}{\partial x} \times \frac{\partial \mathbf{m}}{\partial y} \right) dx dy \quad (3).$$

In Eq. (3), \mathbf{m} is a normalized magnetization vector; x and y are in plane coordinates. On a discrete spin lattice, Eq. (3) is evaluated by summing over the solid angle Ω of three spins according to the Berg formula^{56,57}. Supplementary Fig. 8 shows the topological charge Q of CrTeI as a function of temperature (T) and out-of-plane external magnetic

field (B). Through examining the spin textures under different T and B , we find that the red area with large negative value of Q corresponds to the formation of magnetic skyrmion lattices in CrTeI. Because of the strong DMI, magnetic skyrmion lattices may exist in a large T - B parameter space, with T up to 80 K and B from 1 to 8 Tesla. CrTeCl and CrTeBr also form magnetic skyrmion lattices but in a smaller T - B region (Supplementary Fig. 9). Hence, we recommend CrTeI ML as the most promising 2D platform for the realization of magnetic skyrmions.

In summary, based on systematical first-principles studies on vdW Janus ML CrYX (Y =S, Se, Te; X =Cl, Br, I), we find that CrSX (X =Cl, Br, I) are useful FM semiconductors with high Curie temperatures up to 176 K and large induced magnetic moments on the ligand S^{2-} anions. Remarkably, the long-sought QAHE with a large gap of 19 meV and a sizable valley splitting of 37.9 meV are achieved through the magnetic proximity effect in vdW heterostructures CrSBr/Bi₂Se₃/CrSBr and MoTe₂/CrSBr, respectively. Furthermore, CrTeX (X =Cl, Br, I) may host magnetic skyrmion states under external magnetic fields. Our work unveils the promising multifunctionalities of 2D vdW Janus magnet Cr-based dichalcogenide halides and reveals their potential for diverse applications in topotronic and valleytronic devices.

METHODS

First-principles calculations

Our first-principles calculations based on the density functional theory (DFT) are

performed using the Vienna *Ab initio* Simulation Package with the generalized gradient approximation^{58,59}. Core-valence interactions are described by projector-augmented wave pseudopotentials^{60,61}. We utilize an energy cutoff of 350 eV for the plane-wave expansion and fully relax lattice constants and atomic positions until the force acting on each atom is smaller than 0.01 eVÅ⁻¹. To take into consideration the strong correlation effect among Cr 3*d* electrons, we adopt $U=3.0$ eV and $J_H=0.9$ eV¹⁵. As discussed in Supplementary Note 8, we obtain similar results when different U values are employed. In building vdW heterostructures, we use an inplane lattice constant $a_{BS}=4.16$ Å of the relaxed bulk BS for CrSBr/BS/CrSBr and $a_{MT}=3.55$ Å of MoTe₂ (MT) ML⁶² for MoTe₂/CrSBr. When relaxing structures, the first Brillouin zone is sampled by 12×12×1, 6×6×1, and 12×12×1 Γ -centered Monkhorst–Pack k meshes for CrYX, CrSBr/BS/CrSBr, and MoTe₂/CrSBr, respectively. We add a vacuum space of 12 Å between slabs along the normal axis to eliminate the spurious interactions. To obtain the accurate magnetic anisotropy energies of CrYX that arise from SIA, a very dense Γ -centered Monkhorst–Pack k mesh of 24×24×1 is used to sample the first Brillouin zone and the total energy convergence criterion is set to be 10⁻⁷ eV. Magnetic anisotropy energies are determined by computing the total energy difference with magnetic moments of Cr³⁺ ions being parallel and perpendicular to the plane of the CrYX ML. When calculating magnetic anisotropy energies, SOC is explicitly included in self-consistent loops. To correctly describe the weak interaction across the vdW gap in these heterostructures, we employ the nonlocal vdW functional (optB86b-vdW)^{63,64}. Berry curvatures and chiral edge states are calculated by the wannier90⁶⁵ and

WannierTools ⁶⁶.

DATA AVAILABILITY

All data used in this study are available from the corresponding author upon reasonable request.

CODE AVAILABILITY

The central codes used in this paper are VASP, Wannier90 and WannierTools. The Detailed information related to the license and user guide for these codes are available at <https://www.vasp.at>, <http://www.wannier.org> and <http://www.wanniertools.com>.

ACKNOWLEDGMENTS

This project is supported by NSFC-12104518, NKRDPC-2017YFA0206203, NSFC-92165204 and the Startup Grant of Sun Yat-Sen University (No. 74130-18841290). Work at University of California, Irvine is supported by the U.S. Department of Energy, Office of Science, Basic Energy Sciences, under Award DE-FG02-05ER46237. Calculations are performed at Tianhe-2 and NERSC.

AUTHOR CONTRIBUTIONS

Y. H. and F. X. contributed equally to this work. Y. H. and R. W. conceived the whole project. Y. H. and L. Q. carried out the DFT calculations. F. X. performed the MC simulations. All authors made contribution to the final version of the manuscript.

COMPETING INTERESTS

The authors declare no competing interests.

REFERENCES

- 1 Huang, B. *et al.* Layer-dependent ferromagnetism in a van der Waals crystal down to the monolayer limit. *Nature* **546**, 270 (2017).
- 2 Bonilla, M. *et al.* Strong room-temperature ferromagnetism in VSe₂ monolayers on van der Waals substrates. *Nat. Nanotechnol.* **13**, 289 (2018).
- 3 O'Hara, D. J. *et al.* Room temperature intrinsic ferromagnetism in epitaxial manganese selenide films in the monolayer limit. *Nano Lett.* **18**, 3125 (2018).
- 4 Burch, K. S., Mandrus, D. & Park, J.-G. Magnetism in two-dimensional van der Waals materials. *Nature* **563**, 47 (2018).
- 5 Gong, C. & Zhang, X. Two-dimensional magnetic crystals and emergent heterostructure devices. *Science* **363**, eaav4450 (2019).
- 6 Cortie, D. L. *et al.* Two-Dimensional Magnets: Forgotten History and Recent Progress towards Spintronic Applications. *Adv. Funct. Mater.* **30**, 1901414 (2020).
- 7 Huang, B. *et al.* Emergent phenomena and proximity effects in two-dimensional magnets and heterostructures. *Nat. Mater.* **19**, 1276 (2020).
- 8 Bhattacharyya, S. *et al.* Recent Progress in Proximity Coupling of Magnetism to Topological Insulators. *Adv. Mater.* **33**, 2007795 (2021).
- 9 Jiang, X. *et al.* Recent progress on 2D magnets: Fundamental mechanism, structural design and modification. *Appl. Phys. Rev.* **8**, 031305 (2021).

- 10 Mermin, N. D. & Wagner, H. Absence of Ferromagnetism or Antiferromagnetism in One- or Two-Dimensional Isotropic Heisenberg Models. *Phys. Rev. Lett.* **17**, 1133, (1966).
- 11 Gong, C. *et al.* Discovery of intrinsic ferromagnetism in two-dimensional van der Waals crystals. *Nature* **546**, 265 (2017).
- 12 Tokura, Y., Yasuda, K. & Tsukazaki, A. Magnetic topological insulators. *Nat. Rev. Phys.* **1**, 126 (2019).
- 13 Hou, Y., Kim, J. & Wu, R. Magnetizing topological surface states of Bi₂Se₃ with a CrI₃ monolayer. *Sci. Adv.* **5**, eaaw1874 (2019).
- 14 Hou, Y. & Wu, R. Axion Insulator State in a Ferromagnet/Topological Insulator/Antiferromagnet Heterostructure. *Nano Lett.* **19**, 2472 (2019).
- 15 Hou, Y. S., Kim, J. W. & Wu, R. Q. Axion insulator state in ferromagnetically ordered CrI₃/Bi₂Se₃/MnBi₂Se₄ heterostructures. *Phys. Rev. B* **101**, 121401 (2020).
- 16 Zhong, D. *et al.* Van der Waals engineering of ferromagnetic semiconductor heterostructures for spin and valleytronics. *Sci. Adv.* **3**, e1603113 (2017).
- 17 Yagmurcukardes, M. *et al.* Quantum properties and applications of 2D Janus crystals and their superlattices. *Appl. Phys. Rev.* **7**, 011311 (2020).
- 18 Zhang, L. *et al.* Recent advances in emerging Janus two-dimensional materials: from fundamental physics to device applications. *J. Mater. Chem. A* **8**, 8813 (2020).
- 19 Lu, A.-Y. *et al.* Janus monolayers of transition metal dichalcogenides. *Nat. Nanotechnol.* **12**, 744 (2017).
- 20 Liang, J. *et al.* Very large Dzyaloshinskii-Moriya interaction in two-dimensional Janus

- manganese dichalcogenides and its application to realize skyrmion states. *Phys. Rev. B* **101**, 184401 (2020).
- 21 Zhang, Y. *et al.* Emergence of skyrmionium in a two-dimensional CrGe(Se,Te)₃ Janus monolayer. *Phys. Rev. B* **102**, 241107 (2020).
 - 22 Cui, Q. R., Liang, J. H., Shao, Z. J., Cui, P. & Yang, H. X. Strain-tunable ferromagnetism and chiral spin textures in two-dimensional Janus chromium dichalcogenides. *Phys. Rev. B* **102**, 094425 (2020).
 - 23 Yuan, J. R. *et al.* Intrinsic skyrmions in monolayer Janus magnets. *Phys. Rev. B* **101**, 094420 (2020).
 - 24 Chaney, G., Ibrahim, A., Ersan, F., Çakır, D. & Ataca, C. Comprehensive Study of Lithium Adsorption and Diffusion on Janus Mo/WXY (X, Y= S, Se, Te) Using First-Principles and Machine Learning Approaches. *ACS Appl. Mater. Interfaces* **13**, 36388 (2021).
 - 25 Abdullahi, Y. Z. *et al.* Ferromagnetic TM₂BC (TM= Cr, Mn) monolayers for spintronic devices with high Curie temperature. *Phys. Chem. Chem. Phys.* **23**, 6107 (2021).
 - 26 Akgenc, B., Vatansever, E. & Ersan, F. Tuning of electronic structure, magnetic phase, and transition temperature in two-dimensional Cr-based Janus MXenes. *Phys. Rev. Mater.* **5**, 083403 (2021).
 - 27 Zhang, C., Nie, Y., Sanvito, S. & Du, A. First-Principles Prediction of a Room-Temperature Ferromagnetic Janus VSSe Monolayer with Piezoelectricity, Ferroelasticity, and Large Valley Polarization. *Nano Lett.* **19**, 1366 (2019).
 - 28 Wu, D., Zhuo, Z., Lv, H. & Wu, X. Two-Dimensional Cr₂X₃S₃ (X = Br, I) Janus

- Semiconductor with Intrinsic Room-Temperature Magnetism. *J. Phys. Chem. Lett.* **12**, 2905 (2021).
- 29 Vatansever, E., Sarikurt, S. & Evans, R. Hysteresis features of the transition-metal dichalcogenides VX_2 ($X = S, Se, \text{ and } Te$). *Mater. Res. Express* **5**, 046108 (2018).
 - 30 Sun, X. *et al.* Room temperature ferromagnetism in ultra-thin van der Waals crystals of $1T-CrTe_2$. *Nano Res.* **13**, 3358 (2020).
 - 31 Purbawati, A. *et al.* In-plane magnetic domains and Néel-like domain walls in thin flakes of the room temperature $CrTe_2$ van der Waals ferromagnet. *ACS Appl. Mater. Interfaces* **12**, 30702 (2020).
 - 32 Li, S. *et al.* Tunable anomalous Hall transport in bulk and two-dimensional $1T-CrTe_2$: A first-principles study. *Phys. Rev. B* **103**, 045114 (2021).
 - 33 Yang, X., Zhou, X., Feng, W. & Yao, Y. Tunable magneto-optical effect, anomalous Hall effect, and anomalous Nernst effect in the two-dimensional room-temperature ferromagnet $1T-CrTe_2$. *Phys. Rev. B* **103**, 024436 (2021).
 - 34 Zhang, X. *et al.* Room-temperature intrinsic ferromagnetism in epitaxial $CrTe_2$ ultrathin films. *Nat. Commun.* **12**, 2492 (2021).
 - 35 Qi, J., Li, X., Niu, Q. & Feng, J. Giant and tunable valley degeneracy splitting in $MoTe_2$. *Phys. Rev. B* **92**, 121403 (2015).
 - 36 Moriya, T. Anisotropic superexchange interaction and weak ferromagnetism. *Phys. Rev.* **120**, 91 (1960).
 - 37 Fert, A., Cros, V. & Sampaio, J. Skyrmions on the track. *Nat. Nanotechnol.* **8**, 152 (2013).

- 38 Xiao, W.-Z., Xu, L., Xiao, G., Wang, L.-L. & Dai, X.-Y. Two-dimensional hexagonal chromium chalcogenides with large vertical piezoelectricity, high-temperature ferromagnetism, and high magnetic anisotropy. *Phys. Chem. Chem. Phys.* **22**, 14503 (2020).
- 39 Banerjee, S., Rowland, J., Erten, O. & Randeria, M. Enhanced Stability of Skyrmions in Two-Dimensional Chiral Magnets with Rashba Spin-Orbit Coupling. *Phys. Rev. X* **4**, 031045 (2014).
- 40 Lin, M.-W. *et al.* Ultrathin nanosheets of CrSiTe₃: a semiconducting two-dimensional ferromagnetic material. *J. Mater. Chem. C* **4**, 315 (2016).
- 41 Zhang, Z. *et al.* Direct photoluminescence probing of ferromagnetism in monolayer two-dimensional CrBr₃. *Nano Lett.* **19**, 3138 (2019).
- 42 Cai, X. *et al.* Atomically Thin CrCl₃: An in-Plane Layered Antiferromagnetic Insulator. *Nano Lett.* **19** (2019).
- 43 Kong, T. *et al.* VI₃—a new layered ferromagnetic semiconductor. *Adv. Mater.* **31**, 1808074 (2019).
- 44 Deng, Y. *et al.* Quantum anomalous Hall effect in intrinsic magnetic topological insulator MnBi₂Te₄. *Science* **367**, 895 (2020).
- 45 Peng, Y. *et al.* A quaternary van der Waals ferromagnetic semiconductor AgVP₂Se₆. *Adv. Funct. Mater.* **30**, 1910036 (2020).
- 46 Zhang, Z., Ni, X., Huang, H., Hu, L. & Liu, F. Valley splitting in the van der Waals heterostructure WSe₂/CrI₃: The role of atom superposition. *Phys. Rev. B* **99**, 115441 (2019).

- 47 Hu, T. *et al.* Manipulation of valley pseudospin in WSe₂/CrI₃ heterostructures by the magnetic proximity effect. *Phys. Rev. B* **101**, 125401 (2020).
- 48 Zollner, K., Junior, P. E. F. & Fabian, J. Proximity exchange effects in MoSe₂ and WSe₂ heterostructures with CrI₃: Twist angle, layer, and gate dependence. *Phys. Rev. B* **100**, 085128 (2019).
- 49 Zhang, H., Yang, W., Ning, Y. & Xu, X. Abundant valley-polarized states in two-dimensional ferromagnetic van der Waals heterostructures. *Phys. Rev. B* **101**, 205404 (2020).
- 50 Wang, J., Lian, B. & Zhang, S.-C. Quantum anomalous Hall effect in magnetic topological insulators. *Phys. Scr.* **T1604**, 014003 (2015).
- 51 Xu, L. *et al.* Large valley splitting in monolayer WS₂ by proximity coupling to an insulating antiferromagnetic substrate. *Phys. Rev. B* **97**, 041405 (2018).
- 52 Moreau-Luchaire, C. *et al.* Additive interfacial chiral interaction in multilayers for stabilization of small individual skyrmions at room temperature. *Nat. Nanotechnol.* **11**, 444 (2016).
- 53 Soumyanarayanan, A. *et al.* Tunable room-temperature magnetic skyrmions in Ir/Fe/Co/Pt multilayers. *Nat. Mater.* **16**, 898 (2017).
- 54 Boulle, O. *et al.* Room-temperature chiral magnetic skyrmions in ultrathin magnetic nanostructures. *Nat. Nanotechnol.* **11**, 449 (2016).
- 55 Yin, G. *et al.* Topological charge analysis of ultrafast single skyrmion creation. *Phys. Rev. B* **93**, 174403 (2016).
- 56 Berg, B. & Lüscher, M. Definition and statistical distributions of a topological number

- in the lattice O(3) σ -model. *Nucl. Phys. B* **190**, 412 (1981).
- 57 Hou, W.-T., Yu, J.-X., Daly, M. & Zang, J. Thermally driven topology in chiral magnets. *Phys. Rev. B* **96**, 140403 (2017).
- 58 Kresse, G. & Furthmüller, J. Efficient iterative schemes for ab initio total-energy calculations using a plane-wave basis set. *Phys. Rev. B* **54**, 11169 (1996).
- 59 Perdew, J. P., Burke, K. & Ernzerhof, M. Generalized gradient approximation made simple. *Phys. Rev. Lett.* **77**, 3865 (1996).
- 60 Blöchl, P. E. Projector augmented-wave method. *Phys. Rev. B* **50**, 17953 (1994).
- 61 Kresse, G. & Joubert, D. From ultrasoft pseudopotentials to the projector augmented-wave method. *Phys. Rev. B* **59**, 1758 (1999).
- 62 Ramasubramaniam, A. Large excitonic effects in monolayers of molybdenum and tungsten dichalcogenides. *Phys. Rev. B* **86**, 115409 (2012).
- 63 Klimeš, J., Bowler, D. R. & Michaelides, A. Chemical accuracy for the van der Waals density functional. *J. Condens. Matter Phys.* **22**, 022201 (2009).
- 64 Klimeš, J., Bowler, D. R. & Michaelides, A. Van der Waals density functionals applied to solids. *Phys. Rev. B* **83**, 195131 (2011).
- 65 Mostofi, A. A. *et al.* wannier90: A tool for obtaining maximally-localised Wannier functions. *Comput. Phys. Commun.* **178**, 685 (2008).
- 66 Wu, Q., Zhang, S., Song, H.-F., Troyer, M. & Soluyanov, A. A. WannierTools: An open-source software package for novel topological materials. *Comput. Phys. Commun.* **224**, 405 (2018).

Correspondence and requests for materials should be addressed to Yusheng Hou.

Figure captions

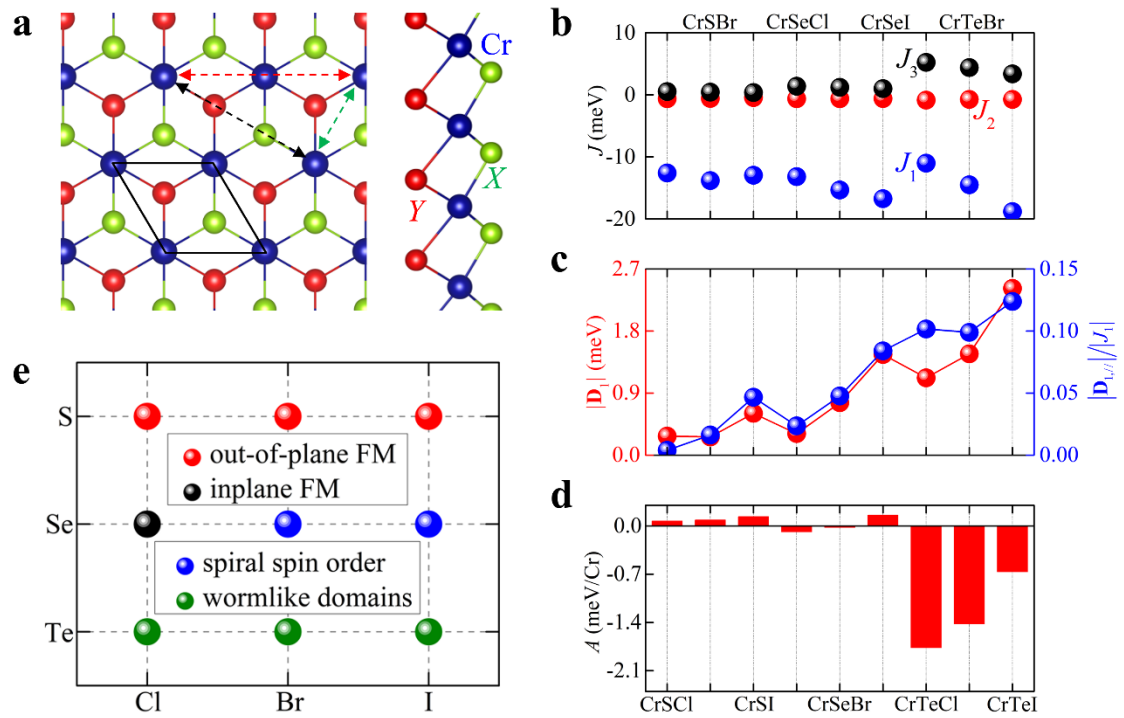


Fig. 1 Crystal structure and magnetic properties of CrYX. **a** Top and side views of the crystal structure. Green, black and red dashed lines show the NN, second-NN and third-NN exchange paths, respectively. **b** Heisenberg exchange parameters J_i ($i=1,2,3$). **c** $|D_1|$ of the NN DM interaction vector \mathbf{D}_1 (red dots) and $|D_{1,||}|/|J_1|$ (blue dots). **d** SIA parameter A . **e** MC simulated magnetic ground states of CrYX.

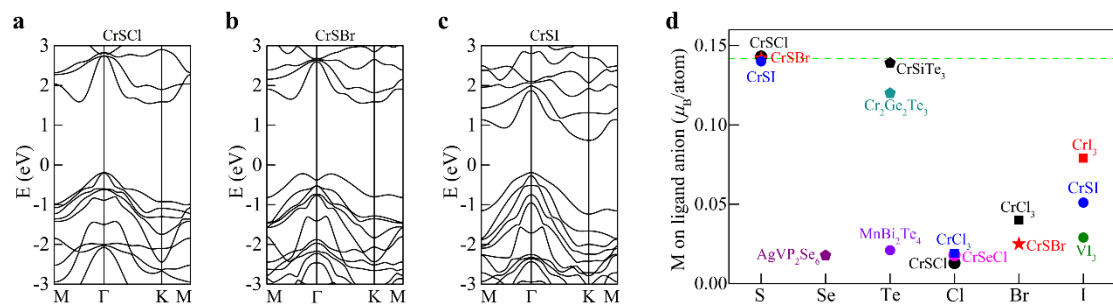


Fig. 2 DFT+U+SOC calculated band structures of a CrSCl, b CrSBr and c CrSI. d

A summary of the DFT calculated induced magnetic moments (M) on the ligand anions of CrSX and other eight representative FM semiconductors. The value of M on S²⁻ ion in CrSBr is highlighted by the green dashed line.

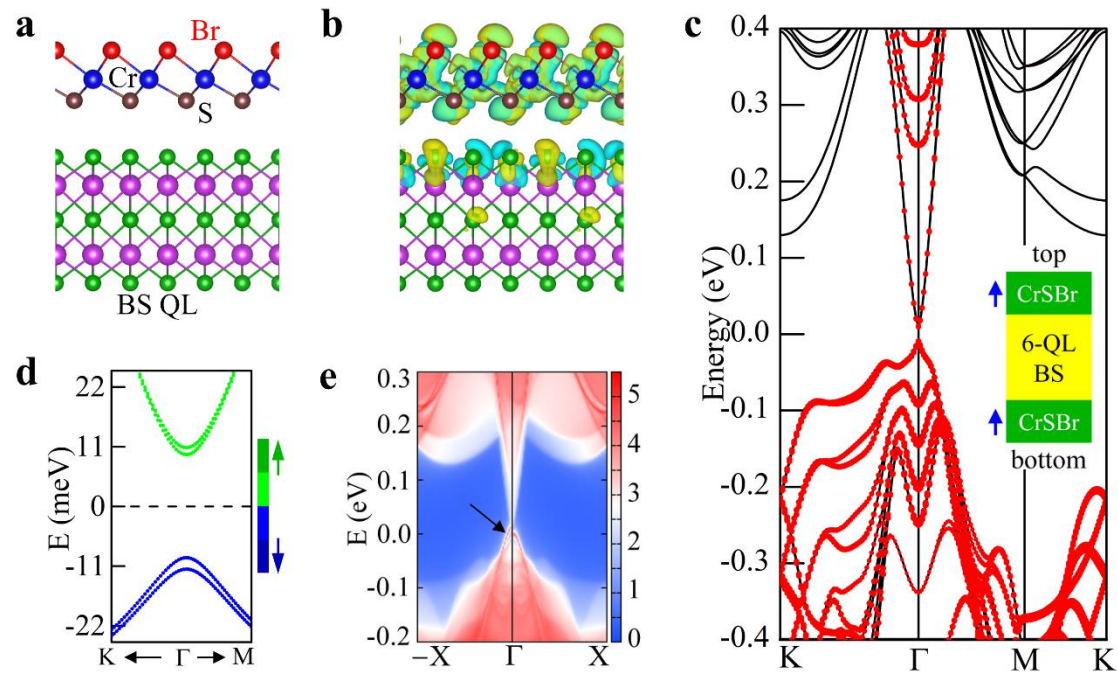


Fig. 3 Electronic and topological properties of CrSBr/BS/CrSBr. a Side view of the stable stacking configuration at the CrSBr/BS interface. **b** The spin polarization at the CrSBr/BS interface. Spin-up and spin-down densities are indicated by the yellow and cyan isosurfaces, respectively. The isovalue surface level of spin density is $6 \times 10^{-6} \text{ e}\text{\AA}^{-3}$. **c** DFT+U+SOC calculated band structure. The inset shows the sketch of the magnetizations (represented by blue arrows) of CrSBr MLs. **d** The four bands near the Fermi level. **(e)** The band structure and the chiral edge state (highlighted by the black arrow) of the one-dimensional CrSBr/BS/CrSBr nanoribbon.

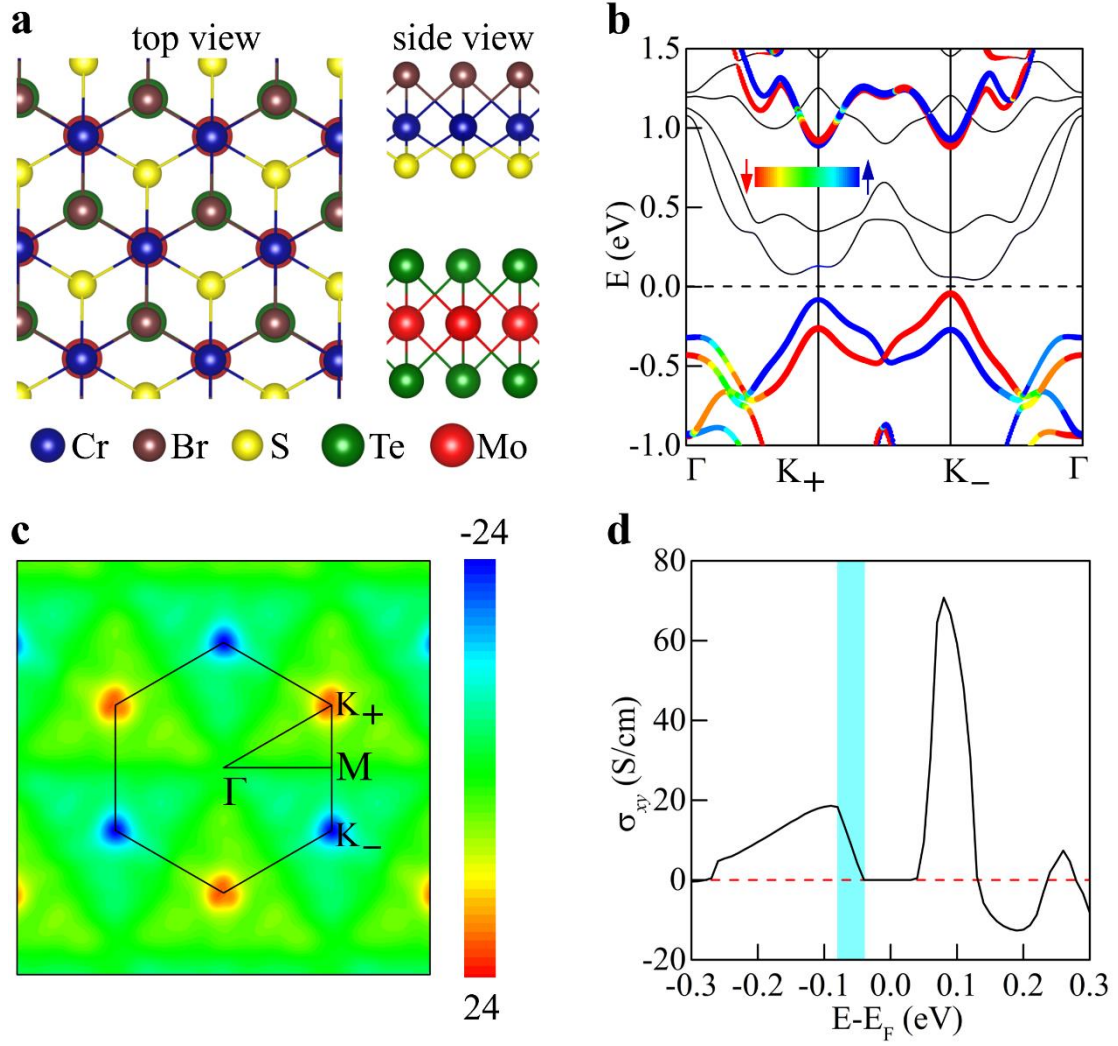


Fig. 4 Electronic and topological properties of CrSBr/MoTe₂. **a** Top and side views of the stable stacking configuration. **b** MoTe₂-projected (colored lines) band structure. Color bar indicates the spin projections. **c** Distribution of Berry curvature (in unit of \AA^2) over 2D Brillouin zone. **d** Dependence of σ_{xy} on the Fermi level. The shaded area denotes the energy window between the two valence-band valley extrema.